

Annealing temperature effects on super duplex stainless steel UNS s32750 welded joints. I: microstructure and partitioning of elements

R. Cervo · P. Ferro · A. Tiziani

Received: 12 October 2009 / Accepted: 8 February 2010 / Published online: 19 February 2010
© Springer Science+Business Media, LLC 2010

Abstract Welding of austenitic-ferritic stainless steels is a crucial operation and all the materials and parameters used in this process must be optimized in order to obtain the suitable corrosion and mechanical properties. Since a great part of super duplex stainless steels is used in very aggressive environment, their corrosion resistance, referred in particular to pitting and crevice corrosion, is an all-important facet in production and processing of this type of steels. Pitting corrosion resistance of super duplex stainless steels welded joints depends on several aspects: microstructure of the bead, elemental partitioning between ferrite and austenite, and the possible presence of secondary phases. For these reasons, a post-weld annealing is generally performed to homogenize the microstructure. The annealing temperature is the most important parameter to be optimized in this heat treatment. In the present work, a comparison between the as-welded and solution-treated joints is carried out. An effort has been made to correlate the main factors that affect pitting corrosion of the welded joints (microstructure, secondary phases, chemical composition of single phases) with the experimental data obtained from corrosion tests. In this first part of the work the results regarding microstructure and partitioning of elements are presented. The phase balance and the austenite morphology are locally upset during submerged-arc welding of UNS S32750. In the fusion zone, the two phases (ferrite and austenite) result to have approximately the same composition regarding Cr, Mo, and Ni content, while nitrogen is heavily concentrated in austenite. After annealing treatment, the austenite volume fraction increases and the

partitioning ratios of elements reach the equilibrium values. The base material results to be less sensitive to annealing treatment than the fusion zone, and the partitioning of elements in the base material is in agreement with previous works reported in the literature.

Introduction

Super duplex stainless steels (SDSS) are corrosion-resistant alloys being widely used in the chemical and petrochemical industries, construction of oil platforms, pulp and paper industries [1]. Since they work in very aggressive environments containing chlorides or other halides, their performance, particularly in term of localized corrosion resistance (pitting and crevice), is a very important subject for researchers and material scientists [2–4].

It is well known that pitting corrosion resistance of SDSS strongly depends on the microstructure characteristics, such as the ferrite/austenite proportion, the presence of intermetallic phases, and elemental partitioning between the austenite and ferrite phases. Such features are all affected by the thermal cycles induced by the welding operation.

In particular, the fusion zone (FZ) and the heat-affected zone (HAZ) are generally characterized by an unbalanced ratio between ferrite and austenite because of the high temperatures reached and the high cooling rates which characterize the welding process [5, 6]. Since the peak temperature in HAZ is much higher than the upper limit of phase balance between δ -ferrite and austenite, most of the γ islands in prior duplex structure dissolve into the δ -ferrite matrix during the heating period. During cooling, in the temperature range between 1300 and 800 °C, the austenite starts to precipitate, both in FZ and HAZ, at the ferrite

R. Cervo (✉) · P. Ferro · A. Tiziani
Department of Management and Engineering, University
of Padova, Stradella San Nicola 3, 36100 Vicenza, Italy
e-mail: riccardo.cervo@unipd.it

grain boundaries due to higher free energy of these locations [7]. Because of the high cooling rate of the weld metal, the ferrite–austenite transformation is inhibited and less austenite will be formed if compared with base material.

Therefore, to achieve the desired microstructure, the heat input must be well controlled during welding of duplex and super duplex stainless steel [7]. Nowacki and Rybicki [8] found in particular that the increase of welding heat input reduces the occurrence of inadmissible welding imperfections in joints, which reduces the costs of testing and repairs. Very low heat inputs lead to high ferrite contents and intense chromium nitride precipitation. On the other hand, high heat inputs and long exposure to temperatures in the 1000–600 °C range may cause precipitation of brittle intermetallic phases such as σ or χ [1].

Another important feature to be considered when corrosion and mechanical properties have to be evaluated in SDSS joints, is the filler metal chemical composition, which influences the FZ microstructure. Usually, filler metals are over alloyed, with 2–4% Ni greater than in the base material (BM) content, to assure a more acceptable austenite content in FZ. In their work, Muthupandi et al. [7] found that nickel enrichment in chemical composition of FZ has a greater influence on the ferrite–austenite ratio than the cooling rate. Tavares et al. [9] studied the corrosion resistance and toughness of a multi-pass weld joint of superduplex stainless steel UNS S32750. The microstructure and chemical composition were determined and correlated to the corrosion and mechanical properties. The root pass was welded with low nickel filler metal and, as a consequence, presented low austenite content and significant precipitation. This precipitation was reflected in the corrosion and mechanical properties. They found that, despite its lower austenite volume fraction (34.2%), the root pass presented a higher Charpy toughness than the filler passes at room temperature; this was attributed to the finer microstructure of the root pass and high oxygen content of the filler passes. Cyclic polarization tests showed that the base metal, root pass, and filler passes present about the same pitting potential ($\sim 1.0 V_{sce}$) and similar PRE (Pitting Resistance Equivalent) indexes. However, the root pass, which contained an excess of ferrite phase and chromium nitride precipitates, was more intensively corroded during the cyclic test. In that work no effort was made in order to study the heat treatment necessary to improve the chemical and mechanical characteristic of the as-welded joints.

Finally, also the partitioning of elements has to be considered in the pitting corrosion behavior of such materials. Austenitic/ferritic stainless steels are characterized by two phases with different chemical compositions and the alloy elements are partitioned in different ways

between them. Thus, the pitting resistance equivalent number (PREN):

$$\text{PREN} = \% \text{Cr} + 3.3\% \text{Mo} + k\% \text{N} \quad (1)$$

with $k = 16 \div 30$, could be evaluated and analyzed for each phase. Since the rapid thermal cycles involved in the welding process, the partitioning of elements in ferrite and austenite is inhibited, and consequently, the pitting corrosion properties of the welded material may be compromised. Perren et al. [3] used a new microelectrochemical method to investigate the individual corrosion behavior of both single phases in super duplex stainless steels. The results showed a good correlation with the empirical PREN value of the corresponding single phases. In particular, both the pitting potentials, evaluated by means of microelectrochemical experiments in pH-neutral lithium chloride electrolyte, and the critical crevice corrosion temperatures showed a good correlation with the PREN of the weaker phase. Even if the annealing temperature in that work was correlated with the PREN of single phases, tests were performed only on the base material so that these kinds of data related to welded joints are still lacking.

In conclusion, welding of DSS and SDSS is often a critical operation [9–11]. The main difficulty is to obtain austenite amounts close to 50% and to avoid the precipitation of deleterious phases [12]. Therefore, it is generally necessary to perform a solution heat treatment on welded joints in order to homogenize the post-welding metastable microstructure. This annealing treatment consists in a heating up to a temperature between 1050 and 1150 °C for 30 min or 1 h, followed by a rapid cooling in order to prevent the precipitation of intermediate phases such as σ , χ , and other detrimental phases [13]. The temperature of this solution heat treatment seems to be a key parameter to determine the final corrosion properties of the welded joint. The main issue is to obtain the best corrosion properties both on the weld metal and on the base material, which are different in terms of chemical composition. To the authors best knowledge, a satisfactory comprehension of the correlation between post-welding heat treatment (PWHT) process parameter and corrosion properties of SDSS is still not reached. An effort was made in this field by Ferro et al. [13] who studied the effect of PWHT on corrosion properties of the DSS SAF 2205. They found a good correlation between the corrosion properties and the secondary austenite morphology which in turn depended on the PWHT parameters.

Aim of this study is to determine the PWHT conditions to obtain the most favorable pitting resistance corrosion properties of the final SDSS welded joints. Special attention is paid to the comparison between the as-welded and the annealed microstructure, the evolution of phase balance and the partitioning of elements for different solution temperatures.

In part I of this work, all the aspects which regard the evolution of the microstructure on UNS S32750 submerged-arc welded joints in relation to the annealing temperature are taken into account to define the appropriate conditions for the PWHT.

In part II the predicted pitting corrosion resistance (in the as-welded and in heat-treated joints) obtained by PREN evaluations, is compared with the actual pitting corrosion behavior, measured through anodic polarization curves and ASTM G48 standard.

Experimental procedure

Materials, welding process, and post-welding heat treatment

Two 15 mm thick plates of UNS S32750 stainless steel (previously solutioned at 1070 °C, then water quenched) were butt welded, with the groove schematically represented in Fig. 1. The nominal compositions of the base and filler metal are shown in Table 1.

It can be noted from Table 1 that the filler metal is enriched in nickel if compared to the base material in order to ensure the correct austenite/ferrite ratio in the FZ.

Welding process was carried out by means of three runs, using submerged-arc welding (SAW) process. The process parameters are listed in Table 2; the heat input was calculated by using Eq. 2 [8]:

$$HI[\text{kJ/mm}] = \eta \frac{V[\text{V}] \times I[\text{A}]}{\text{vel}[\text{mm/s}] \times 1000} \quad (2)$$

where V is the voltage, I is the amperage, vel is the travel speed, and η is a coefficient approximately equal to 0.95 for submerged-arc welding [14].

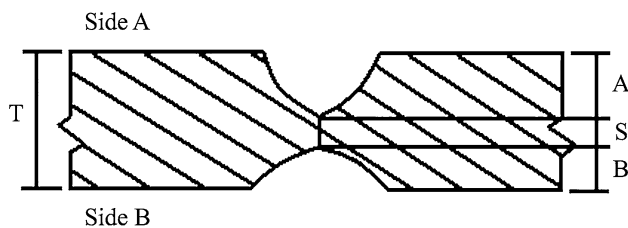


Fig. 1 Schematic representation of the adopted groove ($T = 15$ mm, $A = 4$ mm, $S = 5$ mm, $B = 6$ mm)

Table 1 Chemical composition (wt%) of the materials used in the study

	C	Cr	Cu	Mn	Mo	N	Ni	Si	P	Co	V	Ti	Nb	W	S
Base metal—UNS S32750	0.018	24.8	0.32	0.79	3.85	0.27	6.92	0.22	0.025	—	—	—	—	—	0.001
Filler metal—25 9 4 NL	0.014	25.12	0.096	0.45	4.04	0.228	9.6	0.39	0.014	0.085	0.047	0.005	0.01	0.01	0.0005

After welding, the solution annealing was performed in laboratory furnaces at 1050, 1100, and 1150 °C temperatures for a holding time of 1 h, followed by water quenching. These heat treatments were performed in the “precipitation-free” temperature range.

Metallographic examinations and chemical analysis

Preparation of metallographic sections transverses to the weld bead consisted of silicon carbide paper grinding followed by diamond paste polishing. Beraha's tint etch (80 mL H₂O, 30 mL HCl, and 1 g K₂S₂O₅) was used to reveal the microstructure while oxalic etchant (100 mL H₂O, 10 g oxalic acid, electrolytic 6 V) was used to identify the possible presence of precipitates.

Microstructural investigations were carried out by means of light optical microscopy (LEICA) and environmental scanning electron microscopy (FEI QUANTA 400). The volume fraction of ferrite and austenite was evaluated carefully by means of LOM interfaced with an image analyzer (LEICA QWIN); the final value is the average of at least 12 measurements, each at different zones of the samples.

Chemical analysis of the joints was performed by using an optical spectrometer for chromium, molybdenum, and nickel content; nitrogen content was determined using a LECO oxygen nitrogen analyzer. EDAX GENESIS energy dispersive spectroscopy (EDS) interfaced with ESEM was used to measure the content of substitutional alloying elements in austenite and ferrite (by using a 25 kV accelerating voltage). Each value is an average of more than 10 EDS measurements normalized with respect to the chemical composition using the following equations:

$$c_{\text{El}}^{\gamma} = \frac{c_{\text{El}}^{\text{tot}}}{V^{\gamma}(1 - P_{\text{El}}^{\gamma}) + P_{\text{El}}^{\gamma}} \quad (3)$$

$$c_{\text{El}}^{\alpha} = \frac{c_{\text{El}}^{\text{tot}} P_{\text{El}}^{\gamma}}{V^{\gamma}(1 - P_{\text{El}}^{\gamma}) + P_{\text{El}}^{\gamma}} \quad (4)$$

where $c_{\text{El}}^{\text{tot}}$ is the total content of the analyzed element (El) obtained from chemical analysis in the case of chromium, molybdenum, and nickel, and from LECO in the case of nitrogen; V^{γ} is the volume fraction of austenite and P_{El}^{γ} is the partitioning ratio of the element calculated from experimental data and given by the ratio between the mass fraction of the element in ferrite and the mass fraction of

Table 2 Welding parameters

Weld layer	Side	Filler metal		Current		Volt range [V]		Travel speed range [cm/min]		Average heat input [kJ/mm]	
		Class	Diameter [mm]	Type polarity	Ampere range [A]						
1	A	25 9 4 NL	2.4	DC-EP	340	360	29	31	54	56	1.09
2	A	25 9 4 NL	2.4	DC-EP	390	410	32	34	46	48	1.60
3	B	25 9 4 NL	2.4	DC-EP	540	560	39	40	36	38	3.35

the element in austenite. Such temperature-dependent value was estimated, for nitrogen, on the basis of previous work of Atamert and King [15]. A good agreement between the calculated nitrogen content in single phases and the measurements with different techniques (Wavelength dispersive X-ray spectroscopy WDX, and X-ray diffraction) was verified [16].

Results and discussion

Chemical analysis

Figure 2 shows the macrostructural appearance of a cross-section of the joint.

It can be noted that the first pass is characterized by a very small area, thus, hereafter only the second and the third runs will be considered for investigations. They will be identified as bottom and top pass, respectively. The dilution ratio was calculated both for the total joint (54%) and for each pass (61 and 43% for top pass (TP) and bottom pass (BP), respectively). It can be observed that the dilution ratio of the top pass is higher than the dilution ratio of the bottom pass because of the different thermal inputs used in such zones (Table 2).

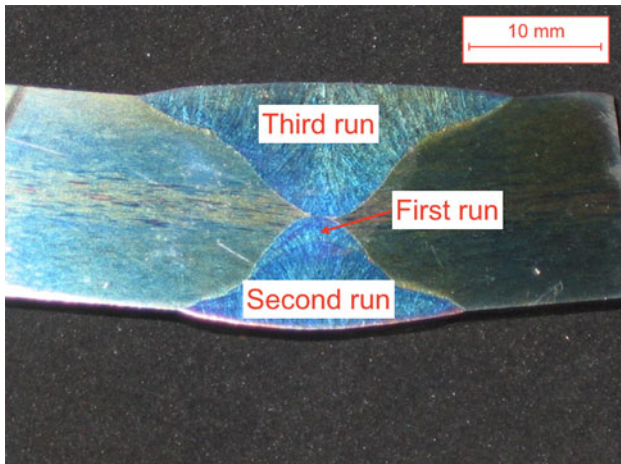


Fig. 2 Macrography of the analyzed multi-pass welded joint showing the three passes performed

Table 3 Chemical analysis (wt%) and calculated PREN of base and weld metal

Sample	Cr ^a	Mo ^a	Ni ^a	N ^b	PREN ₂₀	PREN ₃₀
Top pass	23.91	3.63	7.93	0.23	40.5	42.8
Bottom pass	23.36	3.58	9.28	0.23	39.8	42.1
Base metal	24.32	3.70	6.62	0.27	41.9	44.6

^a Derived from optical spectrometer analysis

^b Derived from LECO analysis

Chemical investigations on top pass, bottom pass, and base metal were performed with an optical spectrometer in order to verify the actual chemical composition of the FZ and BM. Table 3 shows the results obtained and the calculated values of PREN₂₀ and PREN₃₀ (Eq. 1, with $k = 20$ and 30, respectively).

The results collected in Table 3 show that chromium, molybdenum, and nitrogen contents do not change considerably from top to bottom pass; while TP is poorer in nickel than BT. This fact is due to the lower dilution ratio of this last zone compared to upper zone of the bead, thus the effect of the filler metal, in terms of nickel content, is less evident. The values of pitting resistance equivalent number calculated in the as-welded condition are similar for the two passes considered. Chromium, molybdenum, and nitrogen contents in base material are higher than in FZ, and consequently the calculated PREN for the base metal is higher than the one calculated for the bead.

Hereafter, the chemical composition obtained from chemical analysis, that is an “average” value referring to welded zone, was supposed to be constant with the solution temperature; while the “local” chemical composition, referred to austenite and ferrite phases, was supposed to change in relation to the annealing temperature.

Microstructure evolution

The microstructure of the base material in the as-received conditions (austenite volume fraction, $53 \pm 1.94\%$) is shown in Fig. 3.

The microstructure of the as-welded specimen in the FZ was modified as a consequence of the rapid cooling involved in SAW process. The microstructures of top and

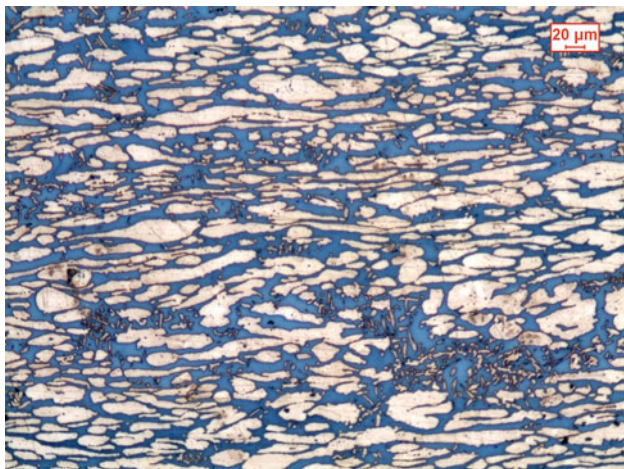


Fig. 3 LOM micrograph of the as-received material showing the typical microstructure constituted by austenite (*white phase*) and ferrite (*dark phase*)

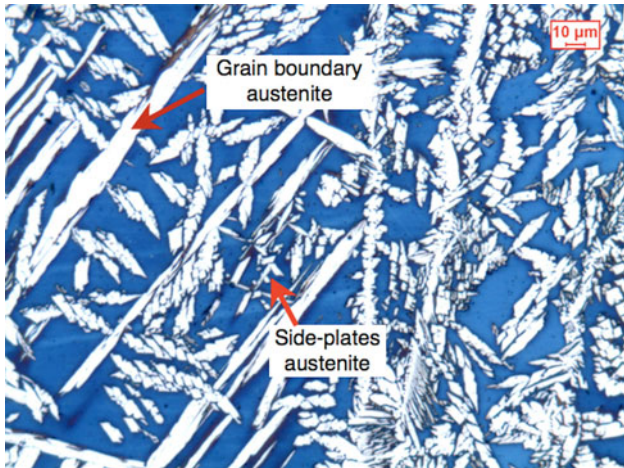


Fig. 4 LOM micrograph of the FZ of the as-welded specimen, showing the types of austenite detected; *dark phase* ferrite, *white phase* austenite

bottom pass are very similar and consist of primary ferrite grain decorated with grain boundary austenite and side-plates austenite (Widmanstätten-type) nucleated from grain boundary austenite (Fig. 4). The austenite volume fractions were 48.1 ± 1.9 and $48.3 \pm 3\%$ in the top and bottom pass, respectively.

Oxalic acid etchant was used to reveal the presence of secondary phases. The possibility of chromium nitride precipitation in HAZ during welding of DSS was indicated in several studies [6, 17, 18]. It is more likely to occur in ferrite phase because the solubility of nitrogen in ferrite drops rapidly with a decrease in temperature. In this case, some chromium-rich and nickel-poor precipitates were observed in HAZ (which had a very limited extension, approximately 100 μm). These precipitates were mainly detected in the

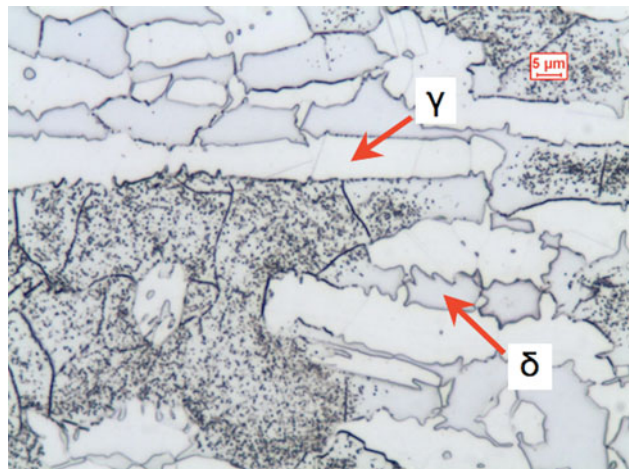


Fig. 5 LOM micrograph of the HAZ of the as-welded specimen showing the presence of precipitates

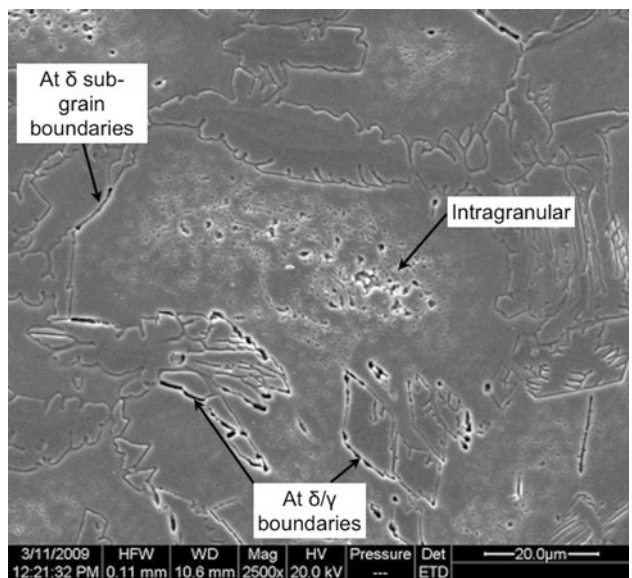


Fig. 6 ESEM micrograph of HAZ (as-welded samples) showing the types of precipitates detected: intragranular, δ/γ boundaries sites, and at ferrite sub-grain boundaries

bottom pass which is characterized by a lower heat input and thus a higher cooling rate (Fig. 5). They are observable inside the ferrite grain, at the ferrite/austenite grain boundaries, and at the ferrite sub-grains boundaries (Fig. 6). It was reported that these secondary phases can have a detrimental effect on corrosion properties [8, 19–21]. Finally, no other kind of precipitate was observed.

A FZ micrograph of the solution-treated specimens is reported in Fig. 7. Compared to the as-welded conditions, both intragranular austenite, precipitated on ferrite grains, and Widmanstätten-type austenite, nucleated at grain boundaries and grown inside the ferrite, were observed [15]; as a consequence, the total austenite volume fraction

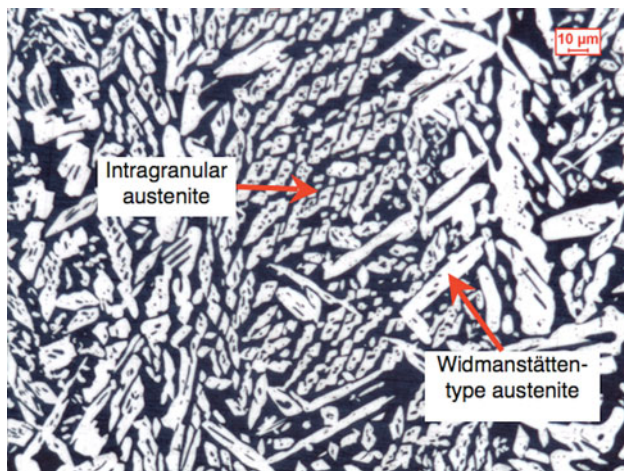


Fig. 7 LOM micrograph of the welded zone of the solution-treated sample ($1100\text{ }^{\circ}\text{C}$) showing the types of austenite formed in relation to annealing treatment (dark phase ferrite, white phase austenite)

Table 4 Experimental austenite volume fractions (%) at different zones of FZ and BM as a function of the annealing temperature

Sample	Fused zone		Base material
	Top pass	Bottom pass	
As-welded	48.1 ± 1.9	48.3 ± 3	53 ± 3.3
ST $1050\text{ }^{\circ}\text{C}$	64.9 ± 3.7	65.8 ± 1.6	55.6 ± 1.2
ST $1100\text{ }^{\circ}\text{C}$	58.8 ± 3.7	62.3 ± 3	49.3 ± 2
ST $1150\text{ }^{\circ}\text{C}$	48.6 ± 0.7	51.8 ± 2	47.8 ± 2.3

in the welded zone increased after solution annealing. Results from image analysis are summarized in Table 4.

The obtained results have shown that FZ is more sensitive than the base material, in terms of austenite volume fractions variations as a function of the solution temperature. Moreover, it can be seen that for the weld metal, the austenite volume fraction increases after solution treatment, if compared with the as-welded specimen. This phenomenon occurs at all the annealing temperatures up to $1150\text{ }^{\circ}\text{C}$. The higher the solution treatment temperature, the lower is the final austenite volume fractions, as justified by the equilibrium diagram reported in [22]. Both the top and the bottom part of the FZ showed a similar phase balance after the heat treatment. Nevertheless, the austenite volume fraction in BM decreases after solution treatment if compared with the as-received conditions. One has to remember that the base material was previously solutioned at $1070\text{ }^{\circ}\text{C}$, thus, the heat-treated and the as-received materials shown the same austenite fraction value at about $1050\text{--}1060\text{ }^{\circ}\text{C}$. In particular, it was found that annealing temperatures at around $1150\text{ }^{\circ}\text{C}$ are much higher for the BM solution treatment.

Regarding the heat affected zones, the precipitates observed in the as-welded joints are not detected in the



Fig. 8 HAZ micrograph of the solution-treated specimen ($1100\text{ }^{\circ}\text{C}$) showing the growth of austenite particles in place of precipitates

solution-treated specimens. This fact is in agreement with the TTT diagram reported in [1] in which it can be seen that for temperatures higher than $950\text{ }^{\circ}\text{C}$ the precipitates are not stable and thus dissolve into the matrix during the heat treatment. Moreover, the growth of austenite particles takes place inside the ferrite grains and starting from grain boundaries austenite, where the precipitates were observed before the solution treatment (Fig. 8); since Ramirez et al. [23] have found a direct relation between the secondary austenite nucleation and chromium nitrides dissolution in HAZ, it can be supposed that the observed precipitates in the specimens analyzed in this work are the same.

EDS analysis

Table 5 collects the normalized chromium, nickel, and molybdenum contents as a function of phase (ferrite, austenite), solution temperature, and area (FZ, BM).

The data collected in Table 5 show that ferrite (both in FZ and BM) becomes richer in chromium and molybdenum and poorer in nickel content as the annealing temperature increases. These results are in agreement with the observations made by Badji et al. [24] and by Tan et al. [25] in a similar material. However, when the solution temperature increases, the increasing in the ferrite volume fraction induces a short of dilution effect and this phase becomes poorer and poorer in ferrite-stabilizer elements.

It can be observed that nickel content is higher in the FZ than in the BM because of the filler metal influence. Finally, EDS analysis shows that chemical composition of austenite and BM is more stable than ferrite and welded metal, respectively. In fact, the bead is a metastable zone if compared with the base material, and it is easy to suppose that the major changing, in terms of phase chemical composition, affects above all the welded joint.

Table 5 Cr, Mo, and Ni contents (wt%) of the specimens analyzed

Sample	Zone	Austenite			Ferrite		
		Cr	Ni	Mo	Cr	Ni	Mo
As-welded	FZ	23.59 ± 0.16	8.81 ± 0.49	3.47 ± 0.11	23.67 ± 0.12	8.41 ± 0.48	3.73 ± 0.61
	BM	23.24 ± 0.10	7.87 ± 0.24	2.93 ± 0.17	25.61 ± 0.23	5.12 ± 0.22	4.62 ± 0.20
ST 1050 °C	FZ	22.70 ± 0.52	9.76 ± 0.40	2.81 ± 0.15	25.40 ± 0.71	6.41 ± 0.58	5.11 ± 0.41
	BM	23.12 ± 0.19	8.02 ± 0.27	2.88 ± 0.35	25.79 ± 0.18	4.90 ± 0.21	4.70 ± 0.24
ST 1100 °C	FZ	22.69 ± 0.51	9.87 ± 0.60	2.72 ± 0.26	25.09 ± 0.65	6.65 ± 0.44	4.97 ± 0.61
	BM	22.97 ± 0.15	7.91 ± 0.33	3.09 ± 0.20	25.84 ± 0.20	5.17 ± 0.13	4.39 ± 0.07
ST 1150 °C	FZ	22.46 ± 0.12	10.09 ± 0.38	2.69 ± 0.19	25.01 ± 0.47	6.84 ± 0.23	4.68 ± 0.18
	BM	23.39 ± 0.25	7.90 ± 0.23	2.98 ± 0.12	25.32 ± 0.14	5.24 ± 0.11	4.48 ± 0.18

ST solution-treated

Partitioning of substitutional elements

Weld metal

Table 6 summarizes the experimentally calculated partitioning ratios (P_{E1}^Y) of molybdenum, chromium, and nickel in the FZ of as-welded and annealed specimens.

It can be noted that P_{E1}^Y values for Mo, Cr, and Ni in the as-welded condition are close to 1, as reported in literature [11]. This is in agreement with the fact that in the FZ the cooling rate is high enough to inhibit the partitioning of elements between austenite and ferrite. After solution treatments, partitioning ratios of Cr and Mo reach the equilibrium values; ferrite enriches in chromium and molybdenum, and becomes poorer in Ni. It can be noted that, molybdenum is characterized by a higher partitioning ratios than chromium, thus it can be considered a stronger ferrite-stabilizer than chromium, as found by Weber et al. for the same material [26].

Base material

Table 7 collects the experimentally calculated partitioning ratios for chromium, nickel, and molybdenum in the BM, both for as-welded and solution-treated samples, and the values derived from the experimental measurements carried out by Tan et al. [25] and Charles [27] for the same material.

Table 6 Experimental partitioning ratios calculated in FZ

Sample	Cr	Ni	Mo
As-welded	1.00	0.96	1.08
ST 1050 °C	1.12	0.66	1.82
ST 1100 °C	1.11	0.67	1.83
ST 1150 °C	1.11	0.68	1.74

ST solution-treated

Table 7 Experimental partitioning ratios in BM

Sample	Cr	Ni	Mo
Experimental			
As-welded	1.10	0.65	1.58
ST 1050 °C	1.12	0.61	1.63
ST 1100 °C	1.12	0.65	1.42
ST 1150 °C	1.08	0.66	1.50
Literature			
ST 1030 °C ^a	1.17	0.62	1.81
ST 1050 °C ^a	1.17	0.64	1.72
ST 1080 °C ^a	1.16	0.66	1.56
ST 1100 °C ^a	1.15	0.67	1.50
ST 1150 °C ^a	1.13	0.70	1.49
ST 1180 °C ^a	1.13	0.72	1.50
ST 1200 °C ^a	1.12	0.73	1.41
ST 1080 °C ^b	1.15	0.65	1.60

ST solution-treated

^a Values reported by Tan et al. [25]^b Values reported by Charles [27]

A comparison between partitioning ratios as a function of annealing temperature reported by Tan et al. [25] and the values found in this study is shown in Fig. 9.

A sufficient agreement was found between the experimental data and the values reported in literature for all the annealing temperatures.

Nitrogen content calculation

Nitrogen weight fraction and its partitioning between ferrite and austenite are fundamental for determining the pitting corrosion behavior of super duplex stainless steels.

Concerning the as-welded conditions of austenitic/ferritic stainless steels, it has been shown by Liljas [28] that at high cooling rates, the interstitial elements controlling the reaction (e.g., nitrogen) are heavily concentrated to the

Fig. 9 Comparison between the partitioning ratios calculated in this work and the values derived from literature versus annealing temperature in BM

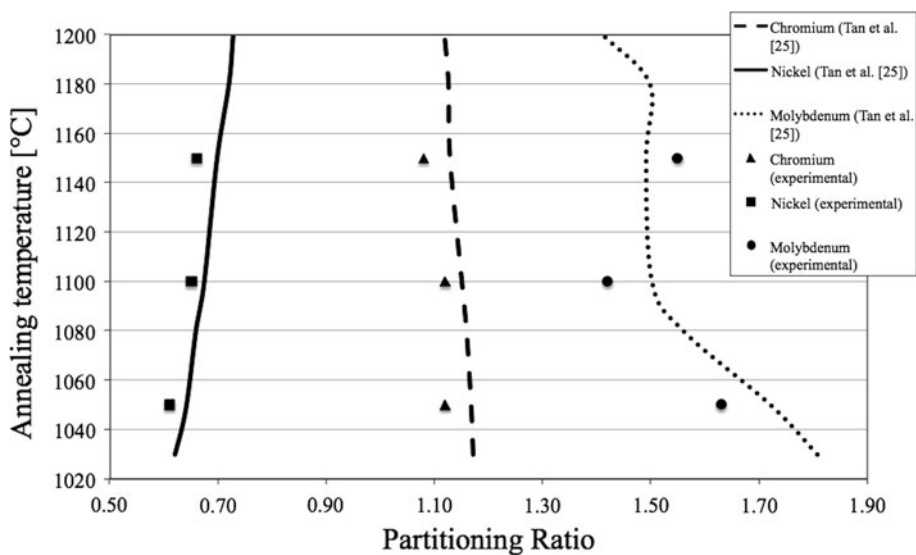
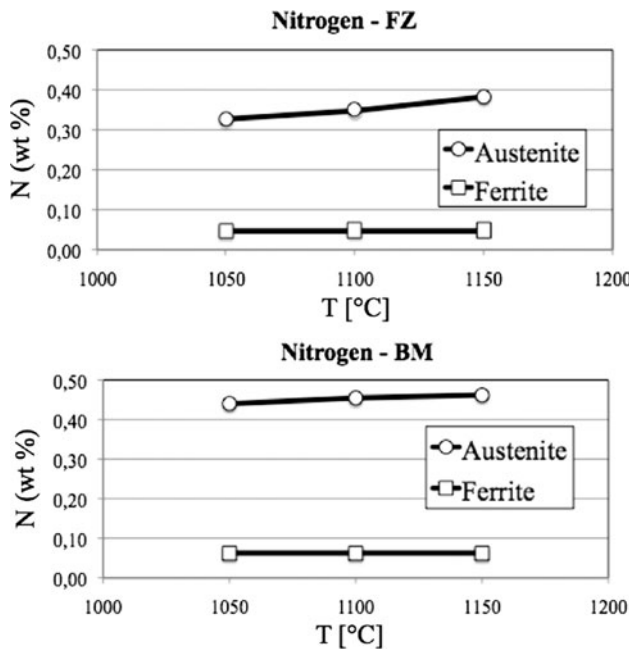


Table 8 Calculated nitrogen content (wt%) for ferrite and austenite at different solution temperatures



Sample	Zone	Austenite	Ferrite
As-welded	FZ	0.42	0.05
	BM	0.46	0.06
ST 1050 °C	FZ	0.33	0.05
	BM	0.45	0.06
ST 1100 °C	FZ	0.35	0.05
	BM	0.47	0.06
ST 1150 °C	FZ	0.38	0.05
	BM	0.49	0.06

austenite. In particular, a nitrogen P_{E1}^γ value of about 1/10 has been measured [28] and used in this study for estimating the nitrogen content in the as-welded conditions. Instead, regarding the annealed specimens, the nitrogen P_{E1}^γ value was assumed to follow the ratio given by Atamert and King [15]: the nitrogen mass fraction in the γ -phase being about seven and eight times higher than in the δ -phase at 1050 and 1250 °C, respectively. For the intermediate annealing temperatures considered in the present study, the value was, in first approximation, linearly interpolated.

Table 8 shows the calculated nitrogen contents for austenite and ferrite at different annealing temperatures, both for BM and FZ (the base metal was previously solutioned at 1070 °C).

It can be observed that austenite becomes richer in nitrogen as the solution temperature increases, while the nitrogen content in ferrite does not substantially change. Moreover, the austenite in the bead seems to be more sensitive to annealing treatments, in term of nitrogen content.

Conclusions

Chemical composition, microstructure, and partitioning of elements were evaluated on UNS S32750 submerged-arc welded joints in the as-welded and annealed conditions.

The following specific conclusions can be drawn:

- Even if a nickel-rich filler metal is used, the phase balance of UNS S32750 is upset during welding as a consequence of the rapid cooling involved in SAW: the austenite amount decreases if compared with BM and

- its morphology changes to grain boundary austenite and side plates Widmanstätten austenite. After annealing treatment, the austenite volume fraction in the FZ increases for all the annealing temperatures, if compared with the as-welded samples; however, the austenite volume fractions decrease as the post-welding annealing temperature increases. The more favorable phase balance in the FZ is reached at annealing temperatures ranging between 1100 and 1150 °C, while for the BM the best phase balance is achieved at lower temperatures (between 1050 and 1100 °C) because of its different composition if compared with the filler metal.
- Some chromium-rich precipitates were detected in the HAZ of the as-welded specimens, which dissolve after annealing treatments above 1050 °C.
 - Because of the high cooling rate induced by the welding process, the experimental (Cr, Mo, Ni) partitioning ratios of the substitutional elements in the FZ of the as-welded specimen are close to 1. Thus, austenite and ferrite have the same chemical composition with the exception of nitrogen content, which is heavily concentrated in austenite. After solution treatment the partitioning ratios in FZ reach the equilibrium values, that is, ferrite enriches in chromium and molybdenum while austenite enriches in nickel and nitrogen. It was found that FZ is more sensitive to P_{E1}^γ variations with annealing temperature than the BM.

Acknowledgements The authors gratefully acknowledge the experimental support provided by Mr. Giacomo Mazzacavallo and Dr. Enrico Della Rovere. Special thanks are also due to Rivit S.p.A. (Caltrano, VI, Italy) for the materials supply and welding.

References

1. Nilsson JO (1992) Mater Sci Technol 8:685
2. Garcia-Garcia DM, Garcia-Anton J, Igual-Munoz A, Blasco-Tamarit E (2006) Corros Sci 48:2380
3. Perren RA, Suter TA, Uggowitzer PJ, Weber L, Magdowski R, Bohni H, Speidel MO (2001) Corros Sci 43:707
4. Perren RA, Suter T, Solenthaler C, Gullo G, Uggowitzer PJ, Bohni H, Speidel MO (2001) Corros Sci 43:727
5. Taban E (2008) J Mater Sci 43:4309. doi:[10.1007/s10853-008-2632-z](https://doi.org/10.1007/s10853-008-2632-z)
6. Migiakis K, Papadimitriou GD (2009) J Mater Sci 44:6372. doi:[10.1007/s10853-009-3878-9](https://doi.org/10.1007/s10853-009-3878-9)
7. Muthupandi V, Bala Srinivasan P, Seshadri SK, Sundaresan S (2003) Mater Sci Eng A358:9
8. Nowacki J, Rybicki P (2005) J Mater Process Technol 164–165: 1082
9. Tavares SSM, Pardal JM, Lima LD, Bastos IN, Nascimento AM, de Souza JA (2007) Mater Charact 58:610
10. Atamert S, King JE (1992) Mater Sci Technol 8:896
11. Bonollo F, Tiziani A, Ferro P (2009) Advances in duplex stainless steels, chap 4. ISTE LTD, London
12. Nilsson JO, Karlsson L, Anderson JO (1995) Mater Sci Technol 11:276
13. Ferro P, Tiziani A, Bonollo F (2008) Weld J 87:298
14. Grong Ø (1997) Metallurgical modelling of welding. The Institute of Materials, Great Britain
15. Atamert S, King JE (1991) Acta Metall Mater 39:273
16. Weber L, Uggowitzer PJ (1995) Proceedings of international symposium on high performance steels for structural applications, ASM, Cleveland, pp 291–298
17. Ogawa T, Koseki T (1989) Weld J 68:181
18. Bonollo F, Gregori A, Tiziani A, Nilsson J-O (1998) A study on microstructural evolution of superduplex steels (SAF 2507) induced by isothermal heat treatment. Proceedings of 11th congress of the international federation for heat treatment and surface engineering, Associazione Italiana di Metallurgia, Milano, vol 3, pp 291–300
19. Liou H-Y, Hsieh R-I, Tsai W-T (2002) Mater Chem Phys 74:33
20. Nilsson JO, Wilson A (1993) Mater Sci Technol 9:545
21. Ha HY, Kwon HS (2007) Electrochim Acta 52:2175
22. Bonollo F, Tiziani A, Ferro P (2009) In: Alvarez-Armas I, Degallaix-Moreuil S (eds) Duplex stainless steels. ISTE LTD, London, p 143
23. Ramirez AJ, Lippold JC, Brandi SD (2003) Metall Mater Trans 34A:1575
24. Badji R, Bouadballah M, Bacoux B, Kahloun C, Bettahar K, Kherrouba N (2008) Mater Sci Technol A496:447
25. Tan H, Jiang Y, Deng B, Sun T, Xu J, Li J (2009) Mater Charact 60:1049. doi:[10.106/j.matchar.2009.04.009](https://doi.org/10.106/j.matchar.2009.04.009)
26. Weber L, Uggowitzer PJ (1998) Mater Sci Eng A 242:222
27. Charles J (1991) Physique 1:3
28. Liljas M (1994) The welding metallurgy of duplex stainless steels. Proceedings of duplex stainless steels 94, Glasgow, Scotland